Acoustic emission analysis of industrial plywood materials exposed to destructive tensile load

Wood Sci Technol (2014) 48:611–631
DOI 10.1007/s00226-014-0628-1

ORIGINAL

Acoustic emission analysis of industrial plywood materials exposed to destructive tensile load

Franziska Ritschel · Yang Zhou · Andreas J. Brunner · Thomas Fillbrandt · Peter Niemz

Received: 22 July 2013 / Published online: 26 March 2014

Abstract Several plywood materials made from spruce wood and, for comparison, solid spruce wood were investigated focusing on the sub-macroscopic damage evolution during tensile loading of the specimens. The destructive tests were simultaneously monitored by the acoustic emission (AE) method and strain field deformation measurement using digital image correlation (DIC). The bilinear interpretation of exponential defect growth identified the start of significant non-linear behavior at 70 % of ultimate strength for all plywood materials. However, already the preceding and more stable damage evolution at lower stress levels has indicated a variation in intensity of the source mechanisms evaluated by AE energy of the detected events. Additional information on the formation of strain field concentration, which correlates with discrete accumulation in AE events and increased spreading in the distribution of AE energy, reveals the complexity of pre-damage due to the variation in cracks' magnitude and timescales involved. The correlation between ultimate tensile strength and damage accumulation below 70 % of ultimate strength is determined, as well as the influence of layered structures on damage size shown by the percentage distribution of AE energy.

F. Ritschel (✉) · P. Niemz
Institute of Building Materials, Swiss Federal Institute of Technology, Zürich, Schafmattstrasse 6, 8093 Zurich, Switzerland
e-mail: fritschel@ethz.ch

Y. Zhou · T. Fillbrandt
University of Freiburg, Werthmannstraße 6, 79085 Freiburg, Germany

A. J. Brunner
Laboratory for Mechanical Systems Engineering, Empa, Swiss Federal Laboratories for Materials Science and Technology, Überlandstrasse 129, 8600 Dübendorf, Switzerland

Introduction

Characterization of damage evolution in wood is a challenge even today. Numerous failure mechanisms have already been extensively documented, especially from various structural elements and load cases. However, since several length scales are involved, such as those introduced by the chemical constituents, cell wall structures, the composition and arrangement of cell types at the microscopic level and also the annual rings at the mesoscopic scale, the complexity of damage progress in wood is hardly traceable (Kollmann 1961; Smith et al. 2003).

Moreover, in the case of wood-based products, such as those studied in the present contribution, the investigated plywood materials, with their layered structure of bonded veneers, induce additional mechanisms at the mesoscopic and macroscopic dimensions. This entails having to analyze the layered material as a continuum matter, while concurrently focusing on its sub-macroscopic structure–function relation (Ivanov and Sadowski 2009). Therefore, one of the most suitable methods is acoustic emission (AE) analysis, because of its sensitivity to elastic waves that have been caused by structural changes at several length scales. Thus, the measurement of AE facilitates multi-scale information on damage progress covering almost the whole specimen volume (Scruby 1987; Beall 2002; Grosse and Ohtsu 2008).

Studies on wood failure using the AE method have already substantiated its nonlinear progress. Furthermore, crack initiation and accumulation, due to load application, have been analyzed for several wood species with respect to the fiber orientation (Debaise et al. 1966; Ansell 1982; Reiterer et al. 2000; Aicher et al. 2001; Ando et al. 2006; Bucur 2006) as well as for several wood-based products (Dunlop 1980; Vun et al. 2005; Brunner et al. 2006; Niemz et al. 2009). Since it is well known that tension loading of wood generates a high degree of AE (Niemz and Lühmann 1992), the present destructive investigations on plywood were performed by tensile loading applied parallel to the grain orientation of the face veneers.

However, since the most crucial issue concentrates on the interpretation of AE parameters, additional measurements, such as optical methods, are needed. For that reason, the AE measurement is combined with the digital image correlation (DIC) monitor on one of the face veneers. This method provides additional information on the materials' behavior by evaluation of the strain field formation (Valla et al. 2010), also revealing indirect information about the underlying plies. In conclusion, the monitoring of tensile tests simultaneously by AE and DIC yields a detailed description of damage evolution due to the layering up of several plywood materials and, by means of a comparison with solid wood, further information is derived.

The present study focuses on the characterization of damage progress of plywood materials during tensile load by taking a closer look at the following issues:

- The onset and the accumulation of defects at microscopic scale.
- The changeover from microscopic mechanisms to pre-damage events at larger scale leading to ultimate failure.
- The dynamic in damage increase in terms of defect growth rates.
- The impact of the layered structures (regarding grain orientation of the veneers) on the linear and nonlinear failure behavior.

- The link between the occurrence of damage events prior to failure and the ultimate tensile strength.

Therefore, the AE activity is analyzed as a function of progressive strain and applied stress level. Furthermore, the individual damage events and mechanisms at several length scales and their interaction are focused more detailed by AE energy and complementary DIC analysis.

Material

The present investigation was carried out on several commercial plywood materials with differently layered structures. The basic constituents are the same: industrially produced rotary-cut veneers of spruce glued together with phenol resin (water boiled proof). Altogether, 3-layered and 5-layered plywood materials (EN 14272 2011) consisting of three to six veneer plies (designated as plywood types 3–6), each of 3 mm thickness, were tested (Fig. 1). Plywood type 3 consists of three layers, whereas the grain of the core ply is oriented perpendicular to the surface layers. The basic layer structure of plywood type 4 is similar to that of plywood type 3, but its core contains an additional cross-grained ply (EN 313-2 1999) (Fig. 1). Analogous to the plywood type 3, the structure of plywood type 5 includes an odd number of veneers. Its core layer is oriented long grained, embedded in adjoined cross-plies. Plywood type 6 contains a double core of long grained plies compared to plywood type 5. In accordance with EN 14272 (2011), plywood type 3 and type 4 are

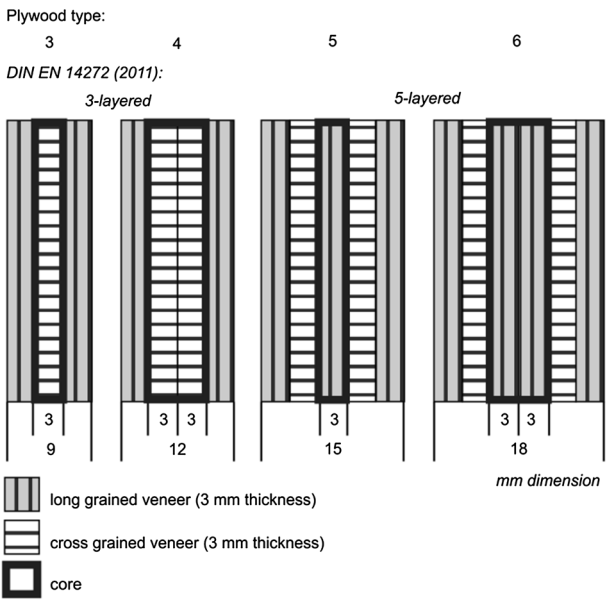

Fig. 1 Layered structure of investigated plywood materials differentiated by their core layup

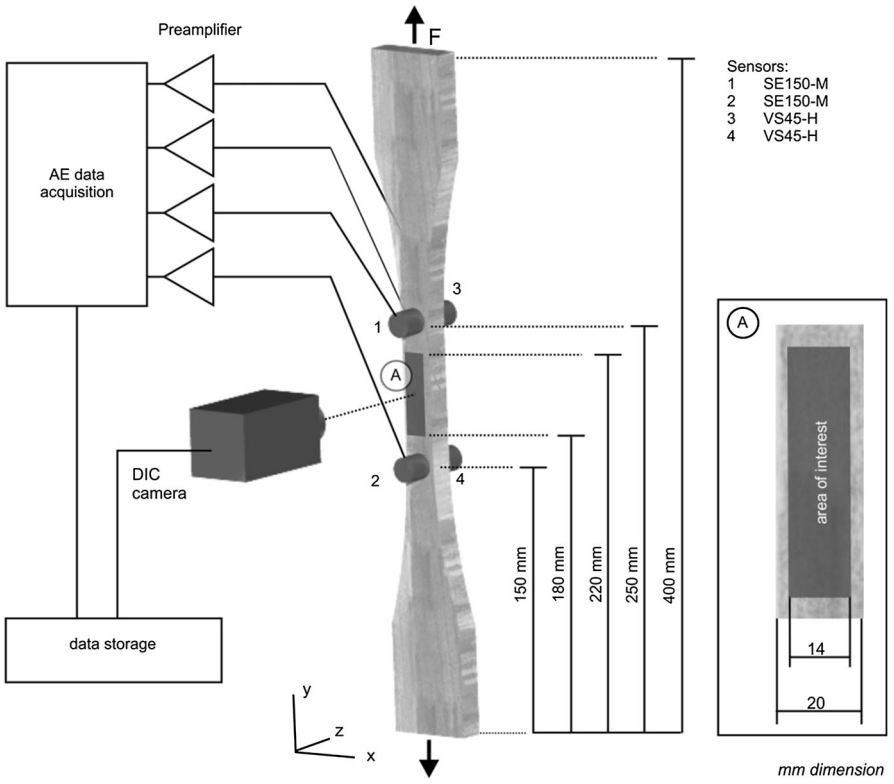

Fig. 2 Schematic of the experimental setup

regarded as 3-layered plywood materials, whereas plywood types 5 and 6 are defined as 5-layered plywood material (Fig. 1).

The specimens (Fig. 2) were prepared in accordance with the German Standard DIN 52377 (1978) for tensile tests on plywood. Tensile load is applied parallel to the grain orientation of the face layer. Moreover, specimens of the same geometry (with a thickness of 9 mm) were made of flawless solid spruce wood (*Picea abies* L.) for purposes of comparison. Overall, eight samples of each material type were tested, which is considered a minimum sample number regarding the natural variation in wood. Nevertheless, eight samples facilitate ranking of the materials properties and obtaining sufficient information on damage evolution for each sample (Fig. 3a). However, it has to be taken into account that the plywood materials are not of the same stock as the solid wood material. Due to the materials' varying origin and history, there are differences in their densities (Table 1). Hence, the correlation of increasing strength with increased raw density applies to plywood, but the solid wood has to be regarded separately. Just for validation, it can be noted that the mechanical properties (Table 1) of the tested solid wood specimens correspond to those reported by several references (e.g., Wagenführ 2000).

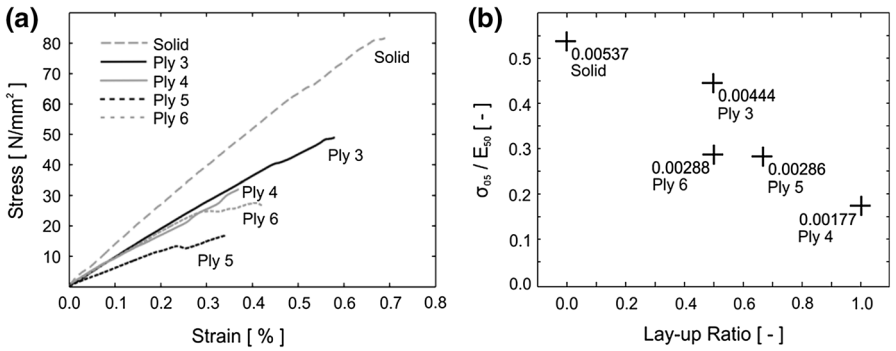

Fig. 3 Average stress–strain *graphs* of the investigated specimens made of several plywood materials and of the solid spruce wood specimens (**a**). Relation between the layup ratio (share of the cross-grained layers to share of the long grained layers) and the low ratio of stress (5 % quantile) to Young's modulus (50 % quantile) of the tested material samples (**b**)

Table 1 Characterization of the investigated material samples

	No. of veneers	Structure and layup ratio (–)	Thickness[a] (mm)	Raw density (kg/m^3)	Moisture content (%)	Young's modulus (GPa)	Strength (MPa)	Ultimate elongation strain (%)
Ply 3	3	I–I	9	500	7.2	9.6	51	0.58[b]
		0.5		(3)		(14)	(11)	(17)
Ply 4	4	I– –I	12	464	7.2	9.0	29	0.37
		1		(4)		(25)	(28)	(30)
Ply 5	5	I–I–I	15	419	7.1	5.6	18	0.34
		0.67		(1)		(34)	(19)	(32)
Ply 6	6	I–I I–I	18	435	7.2	8.0	30	0.42
		0.5		(3)		(40)	(10)	(23)
Solid	1	I	9	400	8.6	13.5	87	0.69
		0		(3)		(10)	(11)	(16)

Mean value (variation coefficient %), no. of samples $n = 8$

[a] Original thickness before planing down by 0.5 mm per surface, each veneer of 3 mm thickness

[b] $n = 7$

Since the selection of the commercial plywood panels was made arbitrarily, more precise information on processed raw material cannot be provided. Therefore, a validation of the material samples is given by the ratio of the tensile strength (5 % quantile) to the Young's modulus (50 % quantile) estimated from the tensile tests. Thereby, the material samples are characterized by the lower ratio of the material's ultimate strength and elastic behavior. Obviously, the correlation between this ratio and the layup ratio (defined as the number of cross-grained plies divided by the number of long grained plies) shows the influence of the cross-grained plies in relation to the material's total thickness (Fig. 3b). Regarding the final tensile

strength parallel to the board orientation (long grain), the cross-grained plies of course have no significant impact on this characteristic property value of the plywood product (EN 14272 2011). Since the present investigation focuses on preceding multi-scaled damage evolution, the ratio of the weak cross-grained plies within the cross section of the specimens is not negligible and thus is taken into account by the layup ratio divergent from the calculation of the thickness to layer ratio proposed by Plath (1974). The quality of the un-planed plywood panels, only defined by the grade of the face veneers, is assigned to class III/III (DIN 68705-2 2003) due to present open defects such as knots and lathe checks. The plywood specimens as well as the solid wood specimens were planed down by 0.5 mm each to create smoother surfaces, in order to improve the coupling of AE sensors to the specimens.

Methods

For quasi-static tensile tests, the specimens were fixed in the universal test machine (type Zwick Roell, load cell calibrated to 100 kN) with mechanically self-tensioning clamping grips. Stress was applied under displacement control with a constant crosshead speed of 2.5 mm/min until the specimen failed (defined by a load drop of at least—5 kN/ms).

The AE measurements were performed with digital AE equipment (type AMSY-6, Vallen Systeme GmbH, Germany) using a sampling rate of 5 MHz. The rearm time was set to 1 ms, and the recording of the AE signals was performed with a resolution of 4,096 samples per set including 200 pre-trigger samples. In each case, two multipurpose sensors of type VS45-H were used, characterized by a relatively flat response displacement in the range of low frequencies between 20 kHz up to 200 kHz, and two 150 kHz resonant sensors of type SE150-M, which are sensitive in the range of 150–450 kHz (Fig. 2). The sensors were coupled to the planed surfaces of the specimens with silicone-free vacuum grease and fixed with metallic spring clamps. Prior to acquisition, the AE signals were amplified by an AEP3 preamplifier (AEP3, gain of 34 dB into 50 Ω, Vallen Systeme GmbH, Germany) and were limited by a (digital) band-pass filter of 30–960 kHz. The threshold was set to the minimum noise-free level 43 dB_{AE}. Noise signals from the grips were excluded by means of two additional guard sensors coupled to both specimen clamps on the testing machine. The AE analysis includes only AE signals (first hit of AE event) recorded prior to the macroscopic failure.

Deformation measurement was performed by the non-contact optical method of two-dimensional DIC. Therefore, during the tensile tests, the area of interest on one wide side of each specimen (Fig. 2 detail A) was monitored with a CCD camera (maximum resolution of 2,048 × 2,048 pixels). The images were taken at a frequency of 2 Hz. Specimens were illuminated by means of a diffuse white light source. However, to enable full-field strain and displacement field measurements, a high-contrast random pattern was applied to the surface of the specimens by airbrushing. Displacements, strains and shear were post-processed by the cross-correlation of a subset in the undeformed image mapped to the corresponding subset

in a deformed image. The processed images have a resolution of 0.12 ± 0.01 mm/pixel. The evaluation focuses predominantly on the strain field formation with respect to the load direction (e_{yy}). Additionally, shear (e_{xy}) was also considered. Both nondestructive methods, AE and DIC measurements, were synchronized by the load signal output of the testing machine.

Results and discussion

Mechanical properties and fracture patterns

First, the several tested (layered) wood materials are regarded as a homogeneous material. Therefore, their mechanical behavior at the macroscopic scale is determined by the stress–strain curves (Fig. 3a). Until shortly before failure, the plywood materials type 3–5 consisting of three, four or five veneers behave in a quasi-brittle manner, just like the solid spruce wood specimens. In contrast, the plywood type 6 shows a distinct plastic deformation at large stresses.

The Young's moduli of the plywood types 3, 4 and 6 are of similar level at 8–10 GPa (Table 1), whereas the plywood type 5 has the lowest Young's modulus of <6 GPa. Obviously, the highest stiffness is determined for the solid specimens with an averaged Young's modulus higher than 13 GPa (Table 1). The variation coefficient of the Young's modulus, which increases with every additional layer in the plywood structure, points to the more complex elastic behavior of the multilayered structures. Certainly, layered structures of more plies degrade the ultimate strength of the final plywood product (Kufner 1966). Accordingly, of all the tested plywood types, type 3 shows the highest strength of approximately 50 MPa and ultimate strains of almost 0.6 % (Table 1). However, in contrast to the elastic behavior of plywood, the ultimate strength linked to fracture formation at the macroscopic scale correlates with the layup ratio of the number of cross-grained plies to that of long grained plies within the plywood's structure. For plywood types 3 and 6, which contain one half long grained plies as cross-grained plies (layup ratio of 0.50), the variation coefficients of ultimate strengths and strains are lower than that of plywood type 4 (layup ratio of 1.00) and type 5 (layup ratio of 0.67). Thus, the increasing share of cross-plies within the layup section provokes variation in failure behavior.

Since the layered structures are exposed to complex loads, and hence, in addition to elongation, shear behavior is also involved (Keylwerth 1954; Norris et al. 1961). However, the averaged results of shear strain of the face veneers are not evident, since the shear strain of the rotary peeled veneers is mainly influenced by the defined growth ring edges on the longitudinal–tangential plane.

In all tested plywood samples, several types of damage occur that are characteristic for plywood (Fig. 4). The final fracture of the plywood specimens passes through several layers, irrespective of their grain orientation, but it does seem to depend on a number of structural features, such as grain orientation among others, and intrinsic flaws or the grade of adhesive layers (Vassiliou 1996). The degraded glue lines and especially the damaged interfaces of the bonded plies lead to

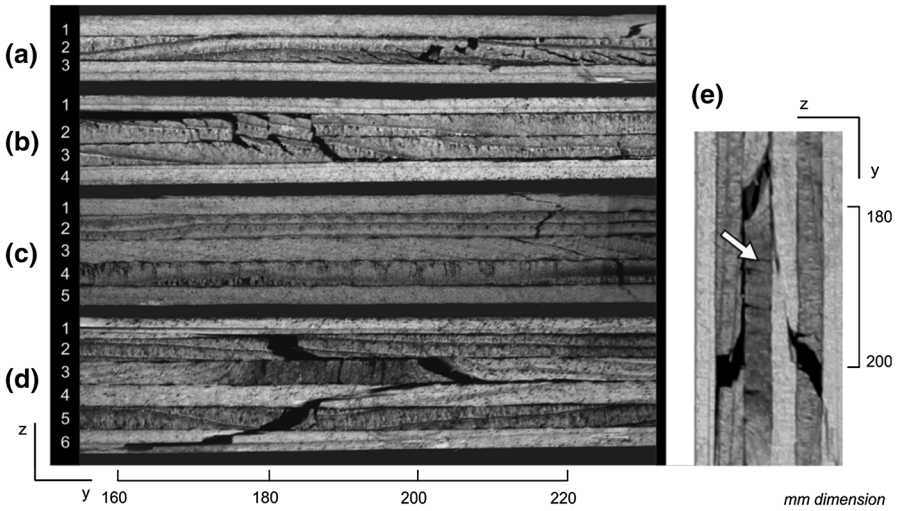

Fig. 4 Exemplary fracture patterns of plywood type 3 (**a**), 4 (**b**), 5 (**c**) and 6 (**d**) that have been exposed to tension. Knot (**e**) in the core layer of plywood type 6 specimen (indicated by *arrow*)

delamination and separation of the adjacent veneers. This was preceded by crack propagation in the cross-grained veneers, formed by shearing the wood structure normal to the grain orientation (Görlacher 2002), where the alignment of growth rings as well as the grain orientation of the enclosing layers plays a role. Hence, cracks opened in the longitudinal–radial plane and cavities of various sizes were created in the radial plane. The fractured layers with longitudinal grain orientation also show shear failures due to the position of the interface of early and latewood.

The damage development of plywood types 3 and 4 are dominated by cracks within their cross-plies, entailing flaws within the associated bond line interfaces, which are mainly caused by rolling shear. Compared to the damage in plywood type 3 (Fig. 4a veneer 2), the crack lengths in the cross-grained layers of plywood type 4 are longer due to its double cross-grained core (Fig. 4b veneers 3 and 4). The most stressed layer in plywood type 5 is its long grained core layer (Fig. 4c, veneer 3). Hence, rolling shear within the cross layers (Fig. 4c veneers 2 and 4) occurred mainly close to the inner bond lines. The fracture of the presented specimen continued by shear and tension failure of the core ply (Fig. 4c, veneer 3). The presented specimen of plywood type 6 (Fig. 4d) shows the most complex failure path, where all damage mechanisms described above occurred, but of even larger size. Compared with plywood type 5, the double long grained core of plywood type 6 is stiffer. Besides, one core layer (Fig. 4d veneer 3) includes an additional flaw in the form of a knot (Fig. 4e), inducing the surrounding crack path formation.

Acoustic emission activity and knee-point evaluation

Since macroscopic failure is preceded by crack initiation and accumulation at the microscopic and mesoscopic scale, analyzing the results from AE measurements

Table 2 Acoustic emission activity and energy of the investigated materials detected by the sensors SE150-M and VS45-H

	AE cumulative activity[a] (10^3)		AE cumulative energy[a] (10^{-5} V^2s)	
	SE150-M	VS45-H	SE150-M	VS45-H
Ply 3	6.2 ± 2.8	7.0 ± 2.7	1.5 (62)	2.6 (57)
Ply 4	5.2 ± 3.8	3.7 ± 2.2	1.2 (60)	1.0 (67)
Ply 5	4.0 ± 2.2	4.5 ± 2.6	0.7 (72)	1.2 (86)
Ply 6	11.1 ± 4.7	13.9 ± 5.7	2.2 (61)	3.0 (48)
Solid	14.6 ± 3.5	16.3 ± 8.5	0.8 (70)	0.8 (86)

Mean value (variation coefficient %), $n = 8$; no. of samples

[a] AE signals of ultimate specimen failure excluded

gives additional information about the damage evolution within the tested plywood structures. For this reason, the AE analysis is limited to AE events preceding the macroscopic failure and ending with an AE signal linked to the highest stress value of the tensile test.

To quantify the damage, the AE activity is summarized by the cumulative numbers of detected AE events. In comparison with the tested plywood samples, the solid wood specimens generated the highest number of AE events (Table 2). Specimens of the plywood type 6 solely showed an AE activity of approximately the same amount. For plywood type 3, even though its specimens have the same physical dimension as the solid wood specimens, only half the AE activity of that for solid wood was measured. Besides the fact that glued wooden structures generally generate a lower number of AE events than solid wood (Gozdecki and Smardzewski 2005), the intrinsic pre-damage due to industrial production of plywood is also of relevance. In particular, lathe checks have already led to a prior release of the material's elastic energy during veneer processing. The AE activity monitored by the two different sensor types (Table 2) is almost the same (Harris and Dunegan 1974).

An overview on damage initiation and accumulation during the load application is given by the cumulative AE activity plotted versus strain (Fig. 5a, b). Thus, the AE activities of the plywood samples are presented normalized to the cumulative AE activity of solid wood. The cumulative AE activity of solid wood roughly follows a linear curve, but with a lower slope closer to failure strain (Fig. 5a). The normalized curves of the plywood samples increase exponentially. Comparing the diagrams that present the AE activities measured by SE 150-M (Fig. 5a) and VS 45-H (Fig. 5b), the curves are almost similar. Furthermore, the normalized cumulative AE activity is set in relation to the stress level defined by the progressive load normalized to the ultimate tensile strength (Fig. 5c, d). Hereby, the curves of plywood types 3 and 4 overlap at stress levels below 50 %. This similarity in normalized AE implies an almost similar damage accumulation at the microscopic scale for both plywood types. At higher stress levels, plywood type 4 shows a slower increase in AE activity than plywood type 3. The number of detected AE signals is probably reduced by the path length between the originating

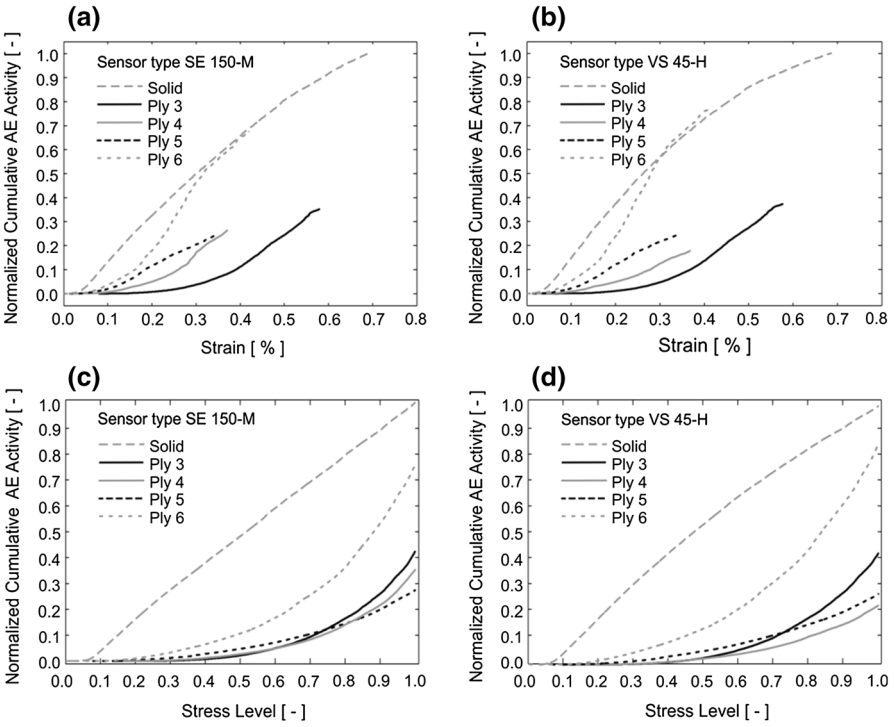

Fig. 5 Normalized cumulative acoustic emission activity of solid spruce and plywood materials in unit of elongation strain measured by sensors of type SE 150-M (**a**) and VS 45-H (**b**). Normalized cumulative acoustic emission activity of solid spruce and plywood materials versus level of ultimate stress measured by sensors of type SE 150-M (**c**) sensor and VS 45-H (**d**). All *curves* are averaged from 8 specimens of each material

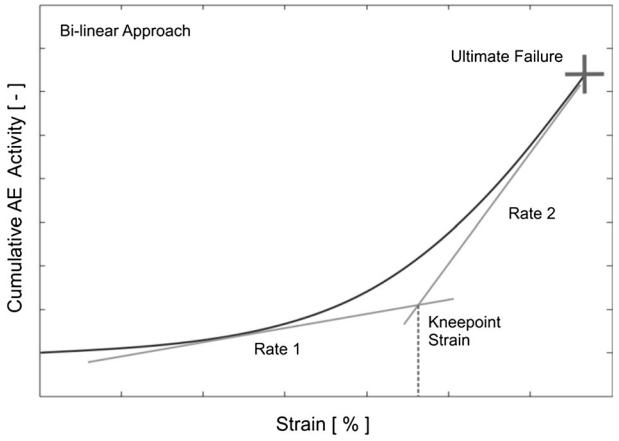

Fig. 6 Principle of bilinear approach to analyze cumulative acoustic emission activity

Table 3 Longitudinal strain and stress level at knee point in Acoustic Emission activity and rates in Acoustic Emission activity of several plywood materials and solid spruce detected by the sensors SE150-M and VS45-H

	Elongation strain at knee point [%]		Stress level at knee point [% of ultimate stress]	1st AE rate (initiation) [s/(0.001 %[a])]		2nd AE rate (initiation) [s/(0.001 %[a])]	
	SE150-M	VS45-H		VS45-H	SE150-M	SE150-M	VS45-H
Ply 3	0.41 (19)	0.39 (17)	74 (4)	39 (45)	53 (38)	258 (24)	291 (29)
Ply 4	0.23 (33)	0.22 (30)	68 (4)	59 (52)	52 (48)	281 (63)	227 (46)
Ply 5	0.20 (28)	0.19 (32)	67 (8)	79 (45)	75 (64)	248 (46)	283 (46)
Ply 6	0.23 (29)	0.22 (27)	75 (21)	132 (17)	191 (30)	531 (49)	694 (53)
Solid				225 (29)	236 (27)	–	–

Mean value (variation coefficient), $n = 8$; no. of samples, *s;* no. of detected AE signals

[a] % elongation strain

source and the sensor location (Aicher et al. 2001) and thus induced reflection and attenuation of the AE signals (Bucur and Feeney 1992).

Since cumulative AE of the plywood materials behave exponentially as a function of time or load, it can be seen by interpreting these curves using the bilinear approach (Fig. 6) that the intersection of both straight lines leads to the so-called knee-point strain value (Kuznetsova et al. 2013). These knee-point values are interpreted to identify the switch from dominating microscopic mechanisms to significant damage onset at a larger scale. For all plywood samples, the knee-point strains were determined from the AE activity progress independently for each sensor type (Table 3). In accordance with the almost similar AE activity curves detected by both sensor types (Fig. 5a, b), the estimated strain values and the related stress levels at the knee points are comparable (Table 3).

Obtained data reveal the onset of significant damage in plywood type 3 at strain values of about 0.4 %. If plywood consists of more than three layers, regardless of their fiber orientation, damage growth on a larger magnitude starts earlier, specifically at strain values of approximately 0.2 % (Table 3). The larger range of elastic behavior of plywood type 3 might be affected by the adhesive and the interface layer, respectively. While the core ply is of the same size as each face ply, the two stiff wood–adhesive interfaces play a more important role than they do in plywood with a higher number of core layers, and respectively with a greater thickness of the core layer (Okuma 1976). However, for all tested plywood materials, the stress levels associated with the knee-point values are almost equal (70 ± 5 %). Entailing a low variation of 4 % in the determination of the knee-point stress levels in the case of plywood types 3 and 4, the additional cross-grained core layer in plywood type 4 induces an earlier acceleration in AE activity growth at 68 % of ultimate stress, whereas the knee point for plywood type 3 was determined at 74 % stress level. Moreover, the knee point in AE activity predicts the start of viscoelastic behavior (Vun et al. 2005), the significant nonlinear behavior of plywood type 6 observed in the stress–strain curve above 20 N/mm^2 (Fig. 3a) correlates with the knee point identified at 75 % stress level (Table 3).

Extending the bilinear approach, the slopes of both straight lines indirectly indicate two rates of flaw growth (however, as a function of strain rather than time) derived from the AE activity rates (Fig. 6). The first AE activity rate characterizes the initial damage accumulation mainly at the microscopic scale, whereas the second AE activity rate, determined from the stress levels of ca. 70 % until the ultimate failure, characterizes the damage increments leading to structural changes at the layup's mesoscopic and macroscopic scales. Here, the AE activity rates are defined by the number of detected AE events per 0.001 % of the progressive strain (Table 3).

Among all tested plywood materials, the initial (first) AE activity rate rises with almost every additional ply, irrespective of the grain orientation of the attached veneer (Table 3). Even bearing in mind the high coefficients of variation, this is still consistent since every additional ply implemented in the material structure offers additional wood matter. Accordingly, additional adhesive joints are being stressed and damaged simultaneously. Hence, flaw development is accelerated. Analogous to the Young's modulus indicating the material behavior at low stress levels within its linear elastic range, the first AE activity rate characterizes the consequences of damage initiation and accumulation within the structural elements of the tested plywood samples at the microscopic scale.

Furthermore, continuing the progressive damage evolution of plywood types 3, 4 and 5 from stress levels >70 %, the second AE activity rate of about 200–300 AE events per 0.001 % strain is more than twice that at low stress levels. Hence, even though crack paths switch to larger scales due to the layered structure, the flaw growth rate of the plywood types 3, 4 and 5 at high stress levels (second AE activity rate) is almost similar to the increase in defects in solid wood. This is due to the increased stress applied to the long grained plies behaving almost similar to the solid wood specimens (Ansell 1982). However, in accordance with its mechanical behavior (Fig. 3a), the second AE activity rate of plywood type 6 is clearly different. In accordance with its distinct plastic deformation on the macroscopic scale, damage growth increases to more than 500 AE events per 0.001 % strain. This is more than double that of the second AE activity rate compared to plywood type 5, which contains only one long grained veneer in the core layer. This is not in contradiction with the distinct plastic deformation already mentioned above, because these structural changes in greater scale are accompanied by an increased number of damages of smaller size.

In conclusion, the damage accumulation within the initial state of destruction below the knee point is found to be in correlation with the ultimate strength of plywood (Fig. 7). The exception of plywood type 5 is discussed below in more detail.

Acoustic emission intensity and strain field formation

Besides the AE activity summarizing the number of occurring damage events, the AE energy (Eq. 1) of the detected events specifies the intensity of the caused damage. All in all, the destructive tension tests of the plywood materials release a total AE energy yielding almost double that of failing solid wood (Table 2), even though plywood samples generate a lower number of AE events. Again, the only exception is plywood type 5, which released more or less the same AE energy as the

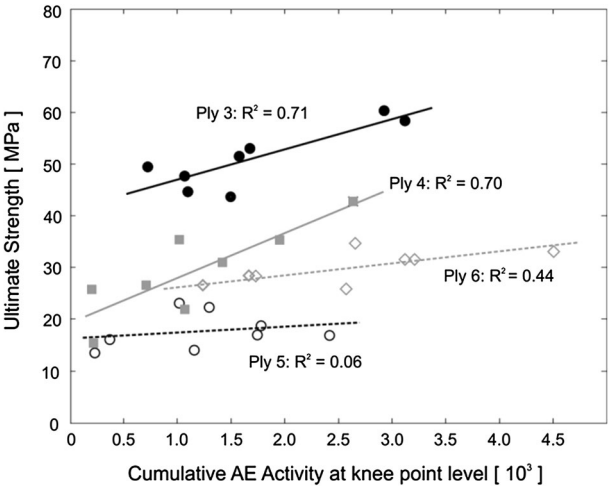

Fig. 7 Correlation between the ultimate strength of plywood materials and their cumulative number of detected acoustic emission events due to development of initial damages

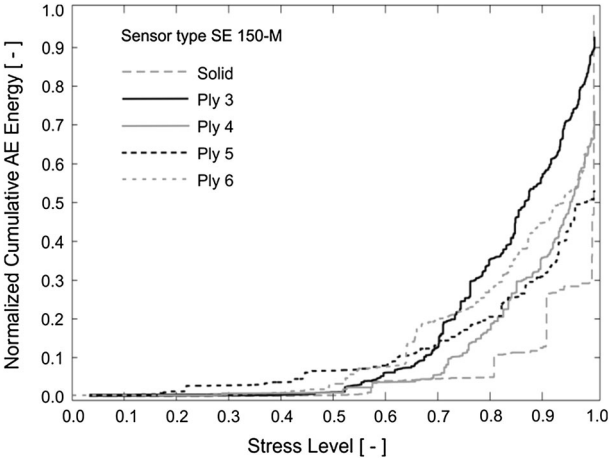

Fig. 8 Acoustic emission energy (detected by sensor type SE 150-M) due to stress level of several plywood materials and of solid spruce

solid spruce wood. First, for a better understanding of the damage processes, the cumulative curves of the AE energies averaged for each material sample are expressed as a function of the applied stress level (Fig. 8). The cumulative AE energy is expressed relative to the absolute AE energy output of each tested material type, and consequently, at stress levels of 100 %, all curves continue by a normalized cumulative AE energy of 100 %.

While the AE activity curve of solid wood increases linearly with increasing stress levels (Fig. 5c), its cumulative AE energy follows an almost exponential increase path (Fig. 8) and hence indicates the nonlinearity in damage evolution

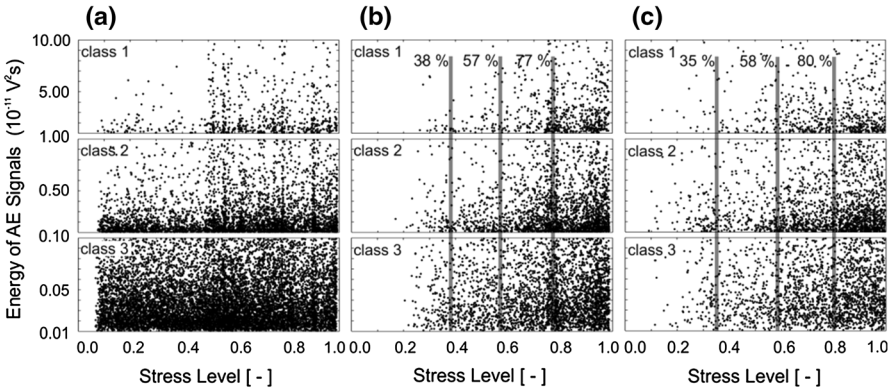

Fig. 9 Acoustic emission energies of the signals against stress level, exemplary presented for one specimen made from solid spruce wood (**a**), plywood type 4 (**b**) and plywood type 5 (**c**). The subplots present the acoustic emission energies of three different limitations: $1 - 10 \times 10^{-11}$ V^2s (*class 1*), $0.11 - 1.0 \times 10^{-11}$ V^2s (*class 2*), $0.01 - 0.10 \times 10^{-11}$ V^2s (*class 3*)

(Nagy et al. 2010). In the case of plywood materials, the exponential increase in normalized cumulative AE activity (Fig. 5c) is accompanied by an almost exponential increase in normalized cumulative AE energy (Fig. 8). At the identified knee-point levels (approximately at a stress level of 70 %), each of the plywood materials released <30 % of their total AE energy, whereas the solid wood released <10 % at the same stress level (70 %). By the time the plywood materials had approached close to 100 % of the stress level, they had already set free more than 50 % of their total AE energies (Fig. 8). In particular, plywood type 3, until shortly before its total fracture, had already released 90 % of its total AE energy, whereas the solid wood generated <50 % of its total AE energy release at comparable stress level.

Since the AE energy of the detected AE events can be used as a measure of damage magnitude (Harris and Bell 1977), the AE signals are classified with respect to their energy content (Fig. 9). This evaluation is performed for AE events detected by the sensor type SE150-M. In accordance with the knee-point level, the evaluation is limited to 70 % stress of ultimate strength. Thus, for investigated materials, the number of signals of each class, relative to the absolute number of AE signals, revealed three main classes; class 1 includes signals with AE energies of $1 - 10 \times 10^{-11}$ V^2s, class 2 contains the signals of $0.11 - 1.0 \times 10^{-11}$ V^2s, and class 3 those of $0.01 - 0.10 \times 10^{-11}$ V^2s. Moreover, for selected specimens, the AE energies of the single AE events are plotted versus applied stress level (Fig. 9a–c). Since the AE energies are within a range of $<10^{-12}$ up to 10^{-8} V^2s, the plots only present the three main AE energy classes already described above.[1]

$$E_i = \int_{t_o}^{t} U^2(t)\mathrm{d}t \tag{1}$$

[1] E_i; acoustic emission energy [V^2s], U; magnitude of acoustic emission signal, t_0; arrival time of acoustic emission signal (t–t_0) duration of acoustic emission signal.

For solid wood, only 2 % of the detected AE signals were due to AE energy class 1. The distribution of AE events within the energy range of class 1 of 10^{-11} – 10^{-10} V^2s increased with increasing stresses (Fig. 9a, class 1). Especially at stresses above 50 %, there are several discrete stress levels identified by accumulations of AE events ranging from 10^{-11} to 10^{-10} V^2s. At these discrete stress levels, AE events of approximately 10^{-10} V^2s are accompanied by a huge number of AE events of lower energy content. The AE energy has been found to be a measure of the damage size, thus the increased distribution of AE energies indicates the variation of damage due to increased stress application (Qi et al. 2010). Hence, it is concluded that at those discrete stress levels yielding a high variation in AE energy in all three energy classes, complex pre-damages are formed. These high variations in AE energy are also consistently represented throughout the plots of AE energy class 2 (Fig. 9a, class 2) and class 3 (Fig. 9a, class 3). Substantially, about 23 % of the detected AE signals for solid wood are counted among AE energy class 2 and 73 % belong to class 3. This fact might correlate with the presence of two main source mechanisms, as already found by Ando (Ando et al. 2006). However, the limitation of the evaluation due to stress levels lower than 70 % of ultimate strength does not completely exclude damages above the microscopic structure. While 73 % of AE signals due to class 3 originated from microscopic damages with very high probability, the events of energy class 2 might be caused by possible pre-damage at a higher scale (Fig. 9a). Altogether, the AE energy release characterizing the damage evolution in solid wood under tension is dominated by a large amount of microscopic damage events generating AE energy contents of $<10^{-12}$ V^2s.

In the case of plywood samples, another percentage distribution in AE energy per event is obtained, which is similar to all plywood types. This correlates with the fact that the failure progress of plywood is dominated not only by microscopic damage mechanisms, but also by flaw growth at the mesoscopic scale due to the layered structure. Hence, more than 10 % of the detected AE events are assigned to AE energy class 1, whereas with increasing stress level, AE energies of approximately 10^{-10} V^2s occur more frequently (Fig. 9b, c, class 1). These 10 % are due to energy class 1 of significantly high energy values, which lead to significant increases in the cumulative AE energy curves of single specimens. This is interpreted as an instable flaw growth that shows the effect of damage evolution due to the crack size range induced by the layered structure. Furthermore, the plywood materials also release a higher share (35–37 %) of signals in AE energy class 2. Within the energy range of class 2, plywood (Fig. 9b, c, class 2) and solid wood (Fig. 9a, class 2) clearly show an accumulation of AE energies beyond 0.3×10^{-11} V^2s. Moreover, the more balanced AE energy distribution of events assigned to energy class 3 (Fig. 9b, c, class 3), and additionally, the minor share of 40–50 % of AE events of class 3, might result from the less microscopic damage initiation within the wooden structure. The growth of intrinsic lathe checks is of larger magnitude and, hence, expected to yield AE events of energy class 1 or 2. Also, matrix cracking is presumed to yield AE energy class 1 and 2. Possibly, fiber breakages within the long grained plies are also reflected in AE energy class 1 and even by AE energy values higher than 10^{-10} V^2s, whereas debonding is likely to appear in the lower range of

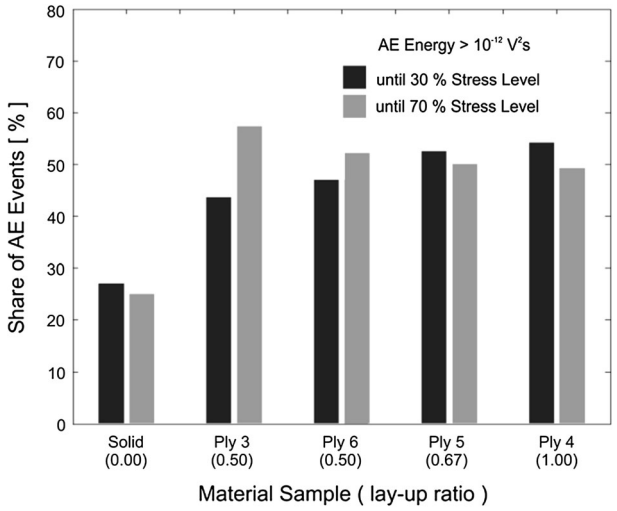

Fig. 10 Influence of layup ratio on the share of acoustic emission events with respect to the acoustic emission energy of $>10^{-12}$ V^2s evaluated until the stress level of 30 % (linear range) and 70 %

AE energy class 3 (Haselbach and Lauke 2003, if wood materials and polymer composites are assumed to behave analogously).

To sum up, the multiple AE energy classes occurring during plywood tensile loading, which altogether show an increasing energy trend of AE events (Fig. 9b, c), result from the cracks progressing through an additional length scale introduced by the layered structure of the plywood. The linear elastic behavior of tensile stressed plywood is mainly dominated by the lower strength of the cross-grained plies. This is verified by the correlation of the ratio of cross-grained plies with the share of events of AE energies above 10^{-12} V^2s (energy class 1, 2 or even above). Thus, with the increasing ratio of cross-grained plies, the share of AE events induce cracks a somewhat larger than micro-cracks (Fig. 10). Above the linear elastic behavior of tensile stressed plywood, until the initiation state runs out, the damage accumulation is less dependent on the layup ratio (Fig. 10). For all plywood materials, there is an almost similar share of AE events inducing cracks larger than micro-cracks at an AE energy of above 10^{-12} V^2s.

Finally, more detailed insight in damage evolution is obtained exemplarily for plywood type 4 and type 5 by correlating the AE energy results (Fig. 9b, c) and the strain field development monitored by the DIC method (Figs. 11, 12). Therefore, sequences of the elongation strain (e_{yy}) and the shear strain (e_{xy}) formation at discrete stress levels as a percentage of the ultimate strength are presented for the selected plywood specimens.

Hence, for the plywood specimen type 4, a first formation of local concentrations in higher elongation strains of approximately 0.3 % shows the pattern of the specimen's weak region (Fig. 11c1) at 38 % of ultimate strength. By further increasing the stress level, a more homogeneous elongation strain formation at 57 % stress level develops (Fig. 11c2). Finally, the pattern of weakness does not reoccur until a stress level of 77 % is reached (Fig. 11c3). In contrast, for plywood type 3,

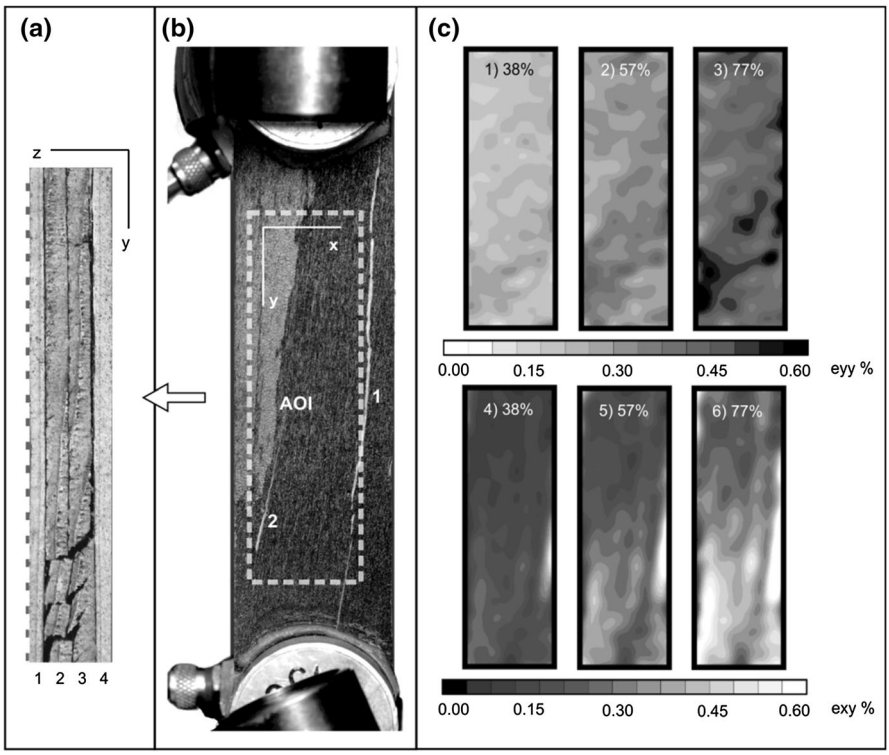

Fig. 11 Visualization of deformation of a selected specimen made of plywood type 4 detailing the fracture pattern through the layered structure (**a**), area of interest monitored by digital image correlation (**b**) including the cracks 1 and 2, progress of strain and shear at several levels of stress (% of ultimate strength) (**c**)

the reoccurring patterns of high strain concentrations already start at about 30 % of ultimate strength and remain until failure (Ritschel et al. 2013). These differences in elongation strain field can be explained by the different importance of the interface of adhesive and wood close to the face veneers. Plywood type 4 consists of a double cross-grained layer with an adhesive in-between. This adhesive interface reinforces the cross-grained core layer normal to the load direction due to the penetration of the adhesive into the intrinsic flaws of both core plies (Okuma 1976). Thus, the core layer dominates the damage evolution. Consequently, both interfaces close to the face veneers are of less relevance. Concurrently, a shear strain of more than 0.1 % is distributed over the entire surface at stress levels below 30 % and further yields first local shear strain concentrations at 38 % stress level, which steadily increases until the specimen fails (Fig. 11c4–6). Hence, at 38 % of ultimate strength, the ultimate elongation strain of the brittle phenol resin glue line between the core and the face veneer is mainly overcome (Serrano 2004; Serrano and Enquist 2005) and shear dominates the failure behavior. The fracture (Fig. 11a) of the specimen plywood type 4 clearly shows the presence of rolling shear, just like the other plywood types.

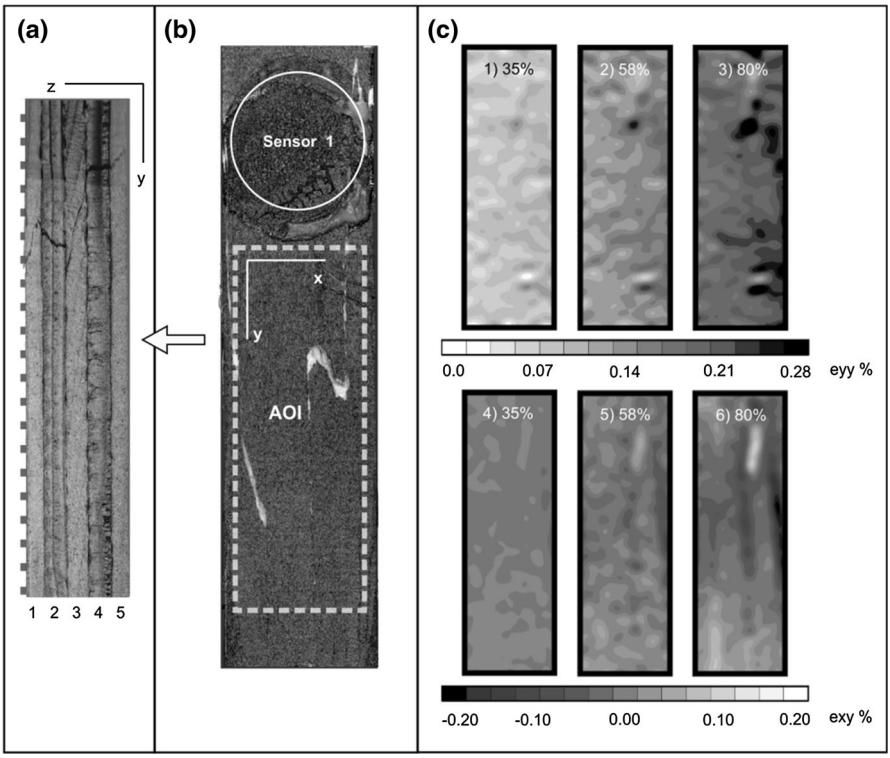

Fig. 12 Visualization of deformation of a selected specimen made of plywood type 5 detailing the fracture pattern through the layered structure (**a**), area of interest monitored by digital image correlation (**b**), progress of strain and shear at several levels of stress (% of ultimate strength) (**c**)

However, it must also be mentioned here, that the presented specimen is an exception among all specimens of plywood type 4, because it forms significant shear strain due to the arrangement of the annual rings cut enclosing the dominant weakness point. Excluding the shear strain of the specimen, the averaged shear strain of plywood type 4 registers 0.10 % (80 % coefficient in variation). Nevertheless, this specimen works well for interpretation of AE results, because the original DIC monitoring photographs enable tracing the initial crack opening of the first macroscopic crack (Fig. 11b, crack 1) caused by the significant pattern in elongation strain and shear strain at a stress level of 77 % observed in the face veneer. This pre-failure in the long grained face ply is also reflected in the AE energy plots of all three AE energy classes, revealing a large distribution of AE energy per event close to the discrete stress level of 77 % (Fig. 9b). Further, a similar pattern in AE energy occurs at a stress level of approximately 95 % (Fig. 9b), which is generated by the formation of the second crack. Finally, the ultimate failure of the specimen brought the first crack to its final size as shown in Fig. 11b (crack 2).

For plywood type 5, the most stressed ply is the long grained veneer in the core. Strains detected by DIC are affected essentially by details of surface deformation

only. However, the surface deformation is also affected by the deformation of the underlying layers. Thus, inhomogeneous patterns of small strains are not replaced by significant concentrations in elongation strain until 80 % stress level (Fig. 12c 1–3). The formation of shear strain concentrations shows a similar trend (Fig. 12c 4–6). The AE measurements, especially the plots of the AE energy per event (Fig. 9c), do not indicate the complex pre-damages. Significant accumulation of AE events at discrete stress levels is absent. Nevertheless, the fracture of the selected specimen shows complex damage through all five plies (Fig. 12a) and implies a very brittle failure behavior of the specimen. It also has to be taken into account that the sensitivity of the sensors is reduced due to the layered structure: number of veneers and presence of adhesive interfaces as well as the increase in the specimen's thickness. However, the AE onset yields a wide spread of AE energy per event within all three classes. Hence, damage initiation and accumulation also includes multiple mechanisms distributed over several length scales due to the intrinsic lathe checks within the veneers and the layup.

All in all, the high variation of AE energies indicates damage mechanisms of several length scales. For plywood types 4, 5 and 6, shear mechanisms dominate the damage progress below the knee-point level (Table 3). However, above the knee point of 70 % of ultimate strength and the correlated strain values above 0.2 %, the long grained face plies play the more important role.

Conclusion

Multi-scaled damage initiation and accumulation from tensile loading was investigated for plywood samples consisting of three, four, five or six veneers of spruce wood. Additionally, specimens of solid spruce wood were tested for comparison purposes. The destructive tests were performed under tension parallel to the board direction at a constant displacement rate synchronously monitored by AE and DIC. Due to the different layup of the plywood samples, differences in damage progression are reflected in the detailed analyzes of AE and DIC results.

- Damage accumulation of plywood is characterized by an exponential increase, expressed in the exponential curve of the cumulative number of AE events with progressive test duration.
- The amount of damage that occurred, measured in numbers of detected AE events, is approximately the same size for plywood types 3, 4 and 5. Significantly, more damage is observed for the plywood type 6. This is in compliance with the plastic deformation already observed at the macroscopic scale in the stress strain graph.
- Two growth rates (number of AE events per 0.001 % elongation strain) are identified in the damage evolution: The initial state of damage growth is represented by the 1st rate, while the 2nd rate specifies the increase in damage progress leading to ultimate failure.
- With increasing number of veneers, the 1st rate also increases. Thus, the initial flaw development is accelerated, because each additional veneer implemented in

the material structure offers additional matter (of wood and adhesive joints) that is stressed and damaged simultaneously.

- For all plywood samples, the 2nd rate of damage increase leading to ultimate failure is nearly quadruple the amount of the initial rate. This is attributed to the fact that microscopic and mesoscopic damage mechanisms act through the veneers and bond lines and coalesce into mesoscopic and macroscopic scale due to layup, finally leading to ultimate failure.
- The state of initial damage accumulation ends at approximately 70 % stress of ultimate strength, whereas shear mechanisms dominate the damage progress below the knee-point level (see Fig. 6) and the long grained face plies play the more important role above the knee-point level.
- The initial AE is affected by the degradation of the natural wooden structure of the veneers by pre-damages (e.g., lathe checks) induced while processing the plywood.
- Within the range of initial damage accumulation (<70 % of ultimate stress), less than 30 % of absolute AE energy is released by all plywood materials. However, multi-scaled damage mechanisms are already included. This is indicated by a high variability in AE energy content of events that covers almost six decades from 0.001 to 100 $\times$ 10^{-11} V^2s.

All in all, the suitability of combining AE measurement and the optical method of DIC has been substantiated. Furthermore, the high time resolution in AE analysis enables more detailed investigations of complex damage mechanisms allowing further verification of parameters encoding the origin of structural changes.

Acknowledgments The authors acknowledge the financial support of the Swiss National Science Foundation under grant SNF-Project 127134. Furthermore, we would like to thank Metsä Wood Schweiz AG for providing the plywood material.

References

Aicher S, Höfflin L, Dill-Langer G (2001) Damage evolution and acoustic emission of wood at tension perpendicular to fiber. Eur J Wood Wood Prod 59:104–116

Ando K, Hirashima Y, Sugihara M, Hirao S, Sasaki Y (2006) Microscopic processes of shearing fracture of old wood, examined using the acoustic emission technique. J Wood Sci 52:483–489

Ansell MP (1982) Acoustic emission from softwood in tension. Wood Sci Technol 16(1):35–57

Beall FC (2002) Overview of the use of ultrasonic technologies in research on wood properties. Wood Sci Technol 36(3):197–212

Bucur V, Feeney F (1992) Attenuation of ultrasound in solid wood. Ultrasonics 30(2):76–81

Bucur V (2006) Acoustics of wood. Springer, Berlin, pp 221–235

Brunner AJ, Howald MT, Niemz P (2006) Acoustic emission rate behavior of laminated wood specimens under tensile loading. J Acoust Emission 24:104–110

Debaise GR, Porter AW, Pentoney RE (1966) Morphology and mechanics of wood fracture. Mater Res Stand 6:493–499

DIN 52377 (1978) Prüfung von Sperrholz; Bestimmung des Zug-Elastizitätsmoduls und der Zugfestigkeit (original in German)

DIN 68705-2 (2003) Sperrholz - Teil 2: Stab- und Stäbchensperrholz für allgemeine Zwecke. (original in German)

Dunlop JI (1980) Testing of particle board by acoustic techniques. Wood Sci Technol 14(1):69–78

EN 313-2 (1999) Sperrholz - Klassifizierung und Terminologie - Teil 2: Terminologie (original in German)
EN 14272 (2011) Sperrholz - Rechenverfahren für einige mechanische (original in German) EN
Görlacher R (2002) Determination of the rolling shear modulus of wood (original in German). Eur J Wood Wood Prod 60(5):317–322
Gozdecki C, Smardzewski J (2005) Detection of failures of adhesively bonded joints using the acoustic emission method. Holzforschung 5(2):219–229
Grosse C, Ohtsu M (eds) (2008) Acoustic emission testing in engineering—basics and applications. Springer, Heidelberg
Harris DO, Dunegan HL (1974) Continuous monitoring of fatigue-crack growth by acoustic-emission techniques. Exp Mech 14(2):71–81
Harris DO, Bell RL (1977) The measurement and significance of energy in acoustic emission. Exp Mech 17(9):347–353
Ivanov IV, Sadowski T (2009) Micromechanical material model of wooden veneers for numerical simulations of plywood progressive failure. Key Eng Mater 399:169–176
Haselbach W, Lauke B (2003) Acoustic emission of debonding between fibre and matrix to evaluate local adhesion. Composi Sci Technol 63:2155–2162
Kollmann F (1961) Rheology and structural strength of wood (original in German). Eur J Wood Wood Prod 19(3):73–80
Kufner M (1966) Permissible stresses in veneer board. (original in German). Eur J Wood Wood Prod 24(11):537–539
Keylwerth R (1954) Actual and possible reduction of anisotropy in composite wood boards (original in German). Eur J Wood Wood Prod 17(6):234–238
Kuznetsova R, Ergun H, Liaw B (2013) Acoustic emission of failure in fiber-metal laminates. In: Büyüköztürk O et al (eds), Nondestructive testing of materials and structures, RILEM Bookseries 6
Nagy E, Landis EN, Davids WG (2010) Acoustic emission measurements and lattice simulations of microfracture events in spruce. Holzforschung 64(4):455–461
Niemz P, Lühmann A (1992) Application of the acoustic emission analysis to evaluate the fracture behavior of wood and derived timber products. Eur J Wood Wood Prod 50(5):191–194
Niemz P, Brunner A, Walter O (2009) Investigation of the mechanism of failure behavior of wood based materials using acoustic emission analysis and image processing. Wood Res 54:49–62
Norris CB, Werren F, McKinnon PF (1961) The effect of veneer thickness and grain direction on the shear strength of plywood. US Forest Products Laboratory, Report No. 1801
Okuma M (1976) Plywood properties influenced by the glue line. Wood Sci Technol 10:57–68
Plath E (1974) Calculation of the thickness/layer ratio of plywood. (original in German). Eur J Wood Wood Prod 32:177–181
Qi G, Wayne SF, Penrose O, Lewis G, Hochstein JI, Mann KA (2010) Probabilistic characteristics of random damage events and their quantification in acrylic bone cement. J Mater Sci Mater Med 21(11):2915–2922
Reiterer A, Stanzl-Tschegg SE, Tschegg EK (2000) Mode I fracture and acoustic emission of softwood and hardwood. Wood Sci Technol 34:417–430
Ritschel F, Brunner AJ, Niemz P (2013) Nondestructive evaluation of damage accumulation in tensile test specimens made from solid wood and layered wood materials. Compos Struct 95:44–52
Scruby CB (1987) An introduction to acoustic emission. J Phys E Sci Instrum 20(8):946–953
Serrano E (2004) A numerical study of the shear-strength-predicting capabilities of the test specimens for wood-adhesive bonds. Int J Adhes Adhes 24(1):23–35
Serrano E, Enquist B (2005) Contact-free measurement and non-linear finite element analyses of strain distribution along wood adhesive bonds. Holzforschung 59(6):641–646
Smith I, Landis E, Gong M (2003) Fracture and fatigue in wood. Wiley, London
Valla A, Konnerth J, Keunecke D, Niemz P, Müller U, Gindl W (2010) Comparison of two optical methods for contactless, full field and highly sensitive in-plane deformation measurements using the example of plywood. Wood Sci Technol 45:755–765
Vassiliou V (1996) Bending strength of thin 3-ply poplar plywood in relation to core veneer joints. Eur J Wood Wood Prod 54(5):360–366
Vun RY, deHoop C, Beall FC (2005) Monitoring critical defects of creep rupture in oriented strandboard using acoustic emission: incorporation of EN300 standard. Wood Sci Technol 39(3):199–214
Wagenführ R (2000) Holzatlas. (original in German) Fachbuchverlag Leipzig. pp 177–178